JOURNAL OF Applied Polymer SCIENCE

Development and characterization of chitosan bionanocomposites containing oxidized cellulose nanocrystals

Vanderlei C. Souza, Eduardo Niehues, Mara G. N. Quadri
Porous Systems Laboratory, Department of Chemical and Food Engineering, Federal University of Santa Catarina—UFSC, Centro Universitário (Trindade), 88040900 Florianópolis, SC, Brazil
Correspondence to: M. G. N. Quadri (E-mail: mara.quadri@ufsc.br)

ABSTRACT: In this research, cellulose nanocrystals (CNs) were extracted from corn cobs by 2,2,6,6,-tetramethylpiperidine-1-oxyl radical-mediated oxidation combined with ultrasonic treatment for the first time. These CNs were then used as a mechanical reinforcement agent and barrier in chitosan-based bionanocomposite films. Birefringence analyses under crossed polarizers indicated the presence of isolated nanocrystals in suspension, which was later confirmed by TEM analysis. The crystallinity index obtained from X-ray diffraction was 92.4%. The incorporation of these nanoparticles into a filmogenic matrix of chitosan made it possible to obtain bionanocomposite films with improved properties. The water-vapor permeability was reduced by 70%, whereas the tensile strength and Young's modulus increased by up to 136 and 224% respectively. The developed films were applied as interleaving of sliced cheese, and the efficiency was assessed by investigation of adhesion between the surfaces and by comparing its properties with two commercial interleaving products (polyethylene (PE), and Greasepel paper (GP)). Concluding, the developed films showed a substantial potential to be exploited as an interleaving film, owing to its excellent mechanical properties, permeability, hydrophobicity, and low surface adhesion compared to pure chitosan, PE, and GP films. © 2015 Wiley Periodicals, Inc. J. Appl. Polym. Sci. **2016**, *133*, 43033.

KEYWORDS: biopolymers and renewable polymers; blends; cellulose and other wood products; mechanical properties; nanoparticles; nanowires and nanocrystals

Received 12 August 2015; accepted 9 October 2015
DOI: 10.1002/app.43033

INTRODUCTION

The increasing global environmental concern regarding the use of nonbiodegradable petroleum-based packaging materials (e.g., polyethylene, polystyrene, and polypropylene) has been encouraging researchers, industries, and governments to design alternative materials made from natural polymers.[1]

In particular, chitosan, the *N*-deacetylated form of chitin, is the only pseudo-natural cationic polymer and, owing to its biocompatibility, biodegradability, toxicity, and antimicrobial activity combined with its cationic character, it is increasingly considered as the greatest potential polymer for obtaining food packaging, especially in the form of biopolymer films.[2,3] However, since chitosan is extracted from shrimp waste, it may not be used for edible films that act as vegetarian food packaging. Although chitosan films have recognized properties that allow them to be applied to food systems, they also have some drawbacks that restrict their use under specific conditions, owing to their low resistance to water-vapor diffusion and relatively low strength tensile, especially in moist environments.[4,5] These are the key research issues that must be solved to enable the application of chitosan films as packaging materials.

A promising strategy to improve the properties of biopolymer films is the incorporation of cellulose nanocrystals (CNs), as they form a percolating network that connects well-dispersed CNs through hydrogen bonds.[6,7] Some studies have been published on the incorporation of CNs in biopolymer matrices, including gluten[8], alginate[9], and starch.[10] The presence of CNs in the polymer matrix provides superior performances such as mechanical and barrier properties, leading to the next generation of biodegradable materials.[7] Chitosan matrices have also been used to prepare bionanocomposite films with different CNs but with the incorporation of plasticizer[11,12] that can potentially cause drastic changes in the mechanical and water-barrier properties of the resulting films. The addition of plasticizer leads to a decrease in intermolecular forces along polymer chains, which improves film flexibility while decreasing the tensile strength and barrier properties of films.[2]

Sulfuric acid hydrolysis is the main process used to extract CNs. This process results in a number of drawbacks, such as corrosivity, environmental incompatibility, and potential degradation of cellulose, thereby providing a comparatively low yield (about 40%) of nanocrystals.[13,14] It is known that the properties and

performance of the CNs as a reinforcement agent mainly depend on the extraction process and the cellulose source.[15] Therefore, obtaining CNs from different process is relevant. Recently, the 2,2,6,6-tetramethylpiperidine-1-oxyl (TEMPO) radical was found to obtain versatile nanocrystals containing carboxylate groups converted from primary hydroxyls of cellulose,[16] which is particularly useful for applications in the nanocomposites as a reinforcement agent. The advantages of using TEMPO oxidation, in comparison to acid hydrolysis, include noncorrosivity as well as high reaction rate, yield, and selectivity with only minimal degradation.[17]

Corn cobs is a agroindustrial waste from the maize crop that contains about 40% of cellulose in its composition.[13] This feature makes the cobs can be investigated as a source of cellulose fibers for the extraction of CNs. In the literature can be found papers on extraction of CNs from corn cobs by acid hydrolysis.[13,18] However, there is not yet any published paper on the extraction of CNs from corn cobs fiber by TEMPO radical-mediated oxidation.

In this research, CNs were extracted from corn cobs, an abundant agroindustrial waste, by TEMPO-radical-mediated oxidation combined with ultrasonic treatment, which were subsequently used as a mechanical reinforcement agent and barrier in chitosan-based bionanocomposite films. One possible application of biopolymers films is in the interleaving of sliced food products, such as cheese. One quality-loss factor of cheese, when sliced, is the adhesion between the slices or between the interleaving and the slices after packaging, making the use of the product by the consumer difficult. As a secondary goal of this research, the developed films were applied as interleaving layers of sliced cheese and its efficiency was assessed by investigating the adhesion between the surfaces and by comparing the film properties (mechanical, water-vapor permeability, hydrophilicity/hydrophobicity, and surface energy) with two commercial interleaving products (polyethylene (PE), and Greasepel paper (GP)).

MATERIALS AND METHODS

Materials

Cellulose fibers (CFs) containing ~90.0, 1.0, and 4.0% cellulose, lignin, and hemicelluloses, respectively, were extracted from the corn cobs following a procedure that has been well described in our previous work.[13] Commercial chitosan from shrimp waste with a deacetylation degree of 98% and high molecular weight was purchased from Polymar (Fortaleza, Ceara, Brazil). Sodium hydroxide (99.0%, P.A., Lafan), hydrogen peroxide (30.0%, P.A., Vetec), sulfuric acid (95.0–98.0%, P.A., Synth), sodium bromide (≥99.0%, P.A., Vetec), sodium hypochlorite (4.0-6.0%, P.A., Sigma–Aldrich), glacial acetic acid (99.7-99.9%, P.A., Nuclear), 2,2,6,6-tetramethylpiperidine-1-oxyl radical (TEMPO, 98.0%, Sigma–Aldrich), and other chemicals were of laboratory grade and used without further purification.

Preparation of CN Suspension

The preparation of a CN suspension was carried out according to a method reported by Ma *et al.*[19] with slight modification. The CFs (10 g) were dispersed in water (192 g) containing TEMPO (0.02 g) and sodium bromide (0.20 g). The reaction started after the addition of 12% NaClO aqueous solution (18 g) and was carried out at room temperature under gentle agitation for 24 h. The pH value was kept at about 10.0–10.5 by adjusting it with 2 wt % NaOH aqueous solution. The reaction was stopped by adding 5 mL ethanol followed by stirring for 20 min. The final product was washed with distilled water by centrifugation at 10,000 rpm for 10 min and then submitted to continuous dialysis using Interlab (São Paulo, SP, Brazil) regenerated cellulose dialysis membranes with 12–14 kDa molecular weight cut off and against distilled water to remove nonreactive groups, salts, and soluble sugars until a neutral pH was reached (after ca. 3 days). An oxidized CN slurry (1.0 g) was dispersed in 100 g of water and the solid aggregates in the suspension were disrupted by sonication (sonicator Unique, 19 kHz, 500 W, model DES, São Paulo, Brazil) for 7 min with a 60% output control. Subsequently, they were stored in a refrigerator at a temperature of 4°C. Drops of chloroform were added to the CN suspension to protect the sample against microbial growth.

Preparation of the Bionanocomposite Films

Chitosan (1% w/w) was dispersed in an aqueous solution of glacial acetic acid (1% v/w) under vigorous stirring at room temperature.[4] After 4 h, the CNs were added to the chitosan solution to reach final concentrations of 0, 6.5, and 14% (w/w). These bionanocomposite-forming dispersions (BFDs) were named CH, CH-6.5CN, and CH-14CN, respectively. These mixtures were homogenized at room temperature using a rotor–stator homogenizer (Ultra-Turrax, model 252-21; Quimis, Diadema, Brazil) at 22,000 rpm for 30 min.[20] The resulting dispersions were filtered through a 0.4 μm millipore filter paper under vacuum to remove air bubbles in the solution and were poured onto petri dishes (diameter = 15 cm) and dried in an oven (model NT 513-D; Nova Técnica) with air circulation at 30°C for ~48 h. The bionanocomposite film thickness was controlled by the volume of the BFD on the petri dishes. All of the prepared bionanocomposites were prepared with 150 mL of filmogenic solution per petri dish (diameter = 15 cm). Dry bionanocomposite films were peeled off from the casting surface and preconditioned in environmental chambers at 25°C and 55% relative humidity for at least 48 h prior to testing. A digital caliper (model VTC; Stainless Hardened, São Paulo, Brazil, ±0.0005 mm) was used to measure the bionanocomposite thickness at a minimum of 12 different points on the same sample, as described by Souza *et al.*[2]

Application of Bionanocomposite Films as the Interleaving of Sliced Cheese

The films were used as the interleaving of American-style sliced cheese (humidity: 44%; fat: 27%; protein: 26%; salt content: 1.7%), which was purchased from a local market in Florianópolis, SC, Brazil. The selected film was interleaved between the slices of cheese (sections 100 × 25 × 1.6 mm^3) (Figure 1) and kept in a refrigerator at 4°C for 24 h prior to the adhesion between the surfaces being evaluated. Adhesion of the films was determined on the second, third, and fourth slices of cheese, and compared with the adhesion of commercial interleaving films, one based on PE (SRC Manufaturados LTDA, São José,

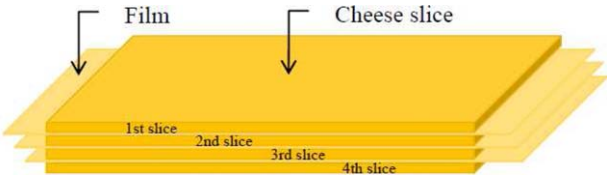

Figure 1. Schematic illustration of the interleaving of sliced cheese. [Color figure can be viewed in the online issue, which is available at wileyonlinelibrary.com.]

SC, Brazil) and the other GP (Fardo Embalagens LTDA, Criciúma, SC, Brazil).

The term adhesion can be understood as the force necessary to break the adhesive bond in order to separate two surfaces that are in contact with one another. This adhesion consists of the sum of interfacial interactions and dissipative energy losses related to the mechanical response of an interface.[21] This value is determined in materials science and the most common method is to use the peel strength test described in Bionanocomposite Film Characterization section.

Analytical Methodology

Characterization of CNs. The CN concentration in the suspension was determined by drying 5 mL suspension at 105°C for 12 h in an air-circulating oven, and the mass was weighed after water evaporation.[15]

The flow birefringence property was used to confirm the presence of isolated CNs in the suspensions. For this purpose, CN suspensions were stirred and observed through a set of two cross-polarized filters in a dark box. Photographs were taken with a Nikon D300s digital camera.

Drops of CN suspensions were placed on glow-discharged carbon-coated TEM grids. The specimen was negatively stained with 2% uranyl acetate for a 10 min period, before it was washed three times prior to complete drying. The samples were observed through a transmission electron microscope (model JEM-2100, TEM, from Japan) operating at 80 kV. The CN dimensions (length and diameter) were determined by a UTHSCSA Image Tool image analyzer program. A minimum of 140 measurements were used to determine the dimensions. Drops of BFDs were also placed on the TEM grids and allowed to evaporate before they were observed under the microscope.

A Perkin–Elmer Infrared spectrophotometer was used to obtain spectra for CFs and CNs. Ground samples were mixed with KBr (sample/KBr ratio, 1/100), after which the mixture was pressed into thin transparent films and analyzed. The experiments were carried out in the range of 500–4000 cm^{-1} with a resolution of 8 cm^{-1} and a total of 32 scans for each sample.

Conductometric titration against 0.04*N* NaOH was carried out to measure the total carboxylate content on the surface of the CFs and CNs. The conductivity was plotted against the volume of the added titrant and carboxyl content (mmol CO_2H/g of CNs or CFs), which was obtained from the difference in inflection points between strong acid and strong base lines.

The crystallinity of the CFs and CNs was studied by an X-ray diffractometer (Panalytical, model Xpert Pro MPD, Brazil) equipped with Cu Kα radiation ($\lambda = 1.5418$ Å) in the 2θ range 10–50°. The operating voltage was 45 kV and the current was equal to 40 mA. The crystallinity index (C_I) was calculated from the heights of the 200 peak (I_{002}, $2\theta = 22.6°$) and the minimum intensity ranged between the 200 and 110 peaks (I_{am}, $2\theta = 18°$), according to the Segal method[22] [eq. (1)]:

$$C_I = \left(\frac{I_{002} - I_{am}}{I_{002}}\right)100 \quad (1)$$

where I_{200} is the peak intensity at the (002) plane ($2\theta = 22.6°$) and I_{am} is the minimum intensity at the valley between the (002) and (110) planes ($2\theta = 18.7°$).

Bionanocomposite Film Characterization. All mechanical tests were performed using a Texture Analyzer (model TA.XP; Stable Microsystems SMD, Godalming, UK) equipped with a 50*N* load cell. Samples were cut into 25-mm-wide and 100-mm-long strips. The tensile strength (σ), elongation percentage (ε) at break point and Young's modulus (Y) were measured uniaxially by stretching the specimen in one direction according to the ASTM D-882 standard.[23] The initial grip separation and crosshead speed were set to 50 mm and 50 mm min^{-1}, respectively.

The water-vapor permeability (WVP) of the films was determined gravimetrically at 25°C, using the ASTM standard method E96-95.[24] Samples of each film in the form of discs (diameter = 70 mm) were fixed with paraffin cell permeation of aluminum, containing anhydrous calcium chloride. These cells were placed in desiccators at 25°C and 75% relative humidity. By increasing the mass of anhydrous calcium chloride (measured in intervals of 24 h for 7 days), it was possible to determine the water vapor transferred through the film according to eq. (2):

$$\mathrm{WVP} = \frac{\Delta m}{\Delta t \times \Delta p \times A} \times e \quad (2)$$

where $\Delta m/\Delta t$ is the weight of moisture loss per unit of time (g s^{-1}), A is the film area exposed to the moisture transfer, e is the film thickness (m), and Δp is the water-vapor pressure difference between the two sides of the film (Pa).

The contact angle (θ) of a water drop deposited onto the film surface is an indicator that enables direct determination of the film surface hydrophobicity or hydrophilicity.[25] The θ measurements at a macroscopic level were determined using the sessile-drop method, in which a droplet of the tested liquid (water and formamide) was placed on the film surface and the drop image was captured by a digital camera connected to a goniometer (Ramé-Hart Model 250, Succasunna, NJ). The θ values were automatically measured and registered by a computer connected to the equipment. Measurements were conducted for 10 s. The contact angles were measured on both sides of the drop and then the average was calculated.

The surface energy of the film was estimated by the geometric mean method.[26] According to the Fowkes equation [eq. (3)], there is a linear relationship between cos θ for the components of the surface tension of the liquid with air and for the

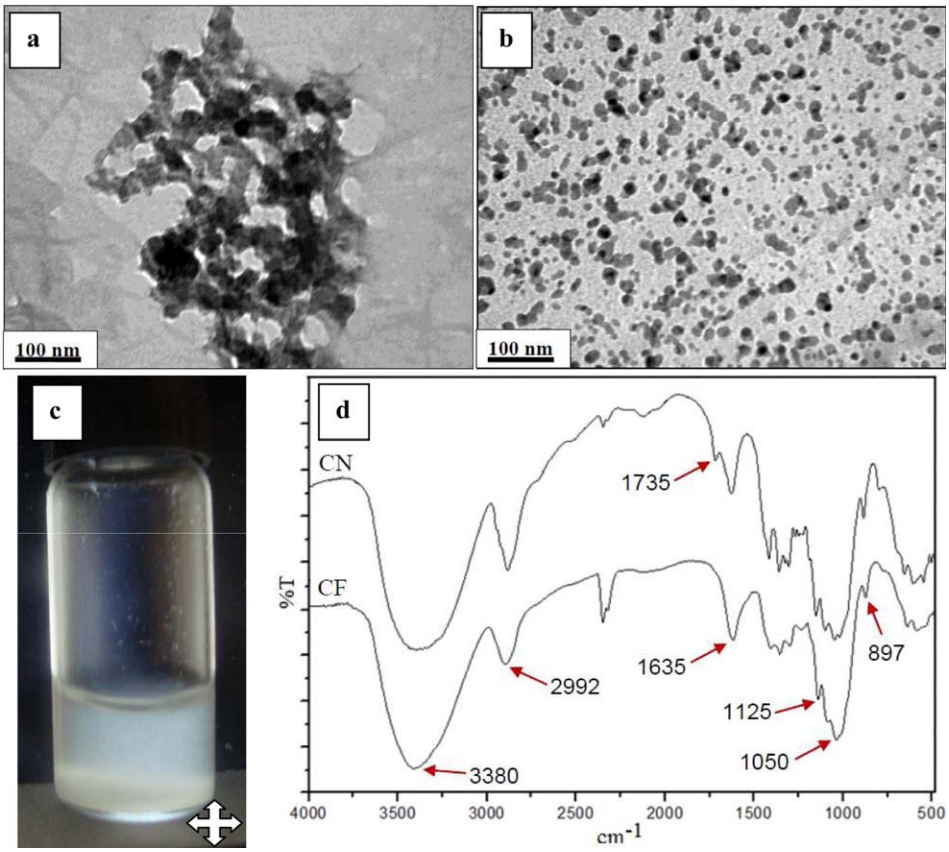

Figure 2. (a) TEM image of aggregated CNs after oxidation treatment, (b) TEM image of isolated CNs after ultrasonic treatment, (c) photograph of the suspension of CNs placed between crossed polarizers, and (d) FTIR spectra of CFs and oxidized CNs. [Color figure can be viewed in the online issue, which is available at wileyonlinelibrary.com.]

components of the surface tension of the solid (in this case, film) with the liquid.

$$\left(\frac{1+\cos\theta}{2}\right)\left(\frac{\gamma_L}{\sqrt{\gamma_L^d}}\right)=\left(\sqrt{\gamma_S^p}\right)\left(\sqrt{\frac{\gamma_L^p}{\gamma_L^d}}\right)+\sqrt{\gamma_S^d} \qquad (3)$$

where γ_L is the total liquid surface tension/energy, γ_L^d is the dispersive component of the liquid surface tension, γ_L^p is the polar component of the liquid surface tension, γ_S^d is the dispersive component of the solid (film) surface tension, and γ_S^p is the polar component of the solid (film) surface tension. The values of the surface tension for the liquids used in these calculations were as follows:[27] water $\gamma_L = 72.8$ mJ m^{-2}, $\gamma_L^d = 21.8$ mJ m^{-2}, $\gamma_L^p = 51.0$ mJ m^{-2}; formamide $\gamma_L = 58.0$ mJ m^{-2}, $\gamma_L^d = 39.0$ mJ m^{-2}, $\gamma_L^p = 19.0$ mJ m^{-2}.

To perform the peel-strength tests, a texturometer (model TA.XP; Stable Microsystems SMD, Godalming, UK) was utilized. The peel test allows us to evaluate the adhesion according to the peel angle (θ) and the width (25 mm) of the film. All tests were performed at a peeling angle of 180° and a peel rate of 300 mm min^{-1} under ambient conditions (24°C, 50% relative humidity), according to the ASTM D-3330 standard.[28]

Statistical Analysis

One-way analysis of variance and Tukey's multiple comparison tests were used to statistically determine the significant differences ($P \leq 0.05$) among the averages, using the software Statistic 6.0 (Statsoft, USA).

RESULTS AND DISCUSSION

Characteristics of the CNs

High-resolution TEM image [Figure 2(a)] revealed that aggregated CNs were obtained after oxidation. The CNs have the tendency to agglomerate, because the cellulose particle size is very small, the specific surface area is very big, and strong hydrogen bonds are established between the crystallites).[29] After being treated by ultrasonication, suspensions of CNs mainly consisted of individual nanoparticles [Figure 2(b)]. This might be attributed to the effect of acoustic cavitation of high-frequency (20–25 kHz) ultrasound in the formation, expansion, and violent collapse of cavities in the aqueous suspension. The violent collapse-induced shockwaves on the surfaces of crystalline cellulose can cause separation. The impact of the sound energy can break the interfaces between the nanocrystals, which are mainly connected to each other through hydrogen bonds. Thus, treatment with sound energy may gradually disperse and disintegrate the nanocrystals.[30,31] In general, the CNs were irregular cylinders or spheres and slightly aggregated with each other. The diameters of the CNs were in the range of 3–17 nm, as measured by UTHSCSA Image Tool software. In our previous work,[13] we observed a similar type of spherical form of nanocrystal isolated from corn cobs by sulfuric acid hydrolysis.

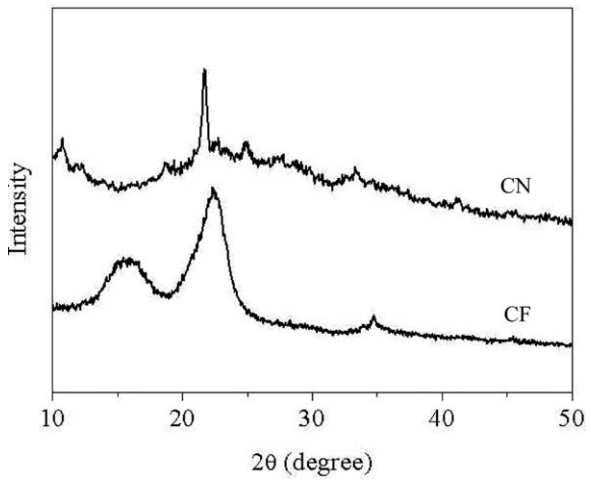

Figure 3. X-ray diffraction images of CFs and oxidized CNs.

Needle like CNs from corn cob have also been reported.[18] The geometric characteristics of the resulting nanocrystals depend on the source and process conditions of cellulose fibers.[13,29] Thus, the same source may also lead to various shaped CNs. The percentage yield of oxidized CNs, with respect to the initial amount of CFs was 60%, which is higher than that prepared by acid hydrolysis (43%),[13] and lower than that of oxidized CNs from jute fibers (about 80%).[16] Furthermore, the values of the CN diameters are comparable to those (3–22 nm) obtained in our previous work.

The CN suspensions viewed under two crossed polarizers presented birefringence flow [Figure 2(c)], highlighting the ability of the CNs to form a chiral nematic liquid-crystalline phase in equilibrium with an isotropic phase.[32] This birefringence phenomenon results from the alignment of nanoparticles[32] and supports the existence of CNs in the suspension.

The FTIR spectra of CFs and oxidized NCs are shown in [Figure 2(d)]. The peaks at 3300–3400 cm^{-1} (O—H stretching vibration) and 2992 cm^{-1} (C—H stretching vibration) are assigned to the adsorbed water.[13] The peaks at 1050 and 897 cm^{-1} are associated with cellulose, the C—O stretching and the C_1—H deformation vibrations of the cellulose,[33] which appeared in all of the spectra. The peak observed at 1125 cm^{-1} corresponds to C—O—C (aryl–alkyl ether).[17] The peak present at 1635 cm^{-1} is due to the presence of C=O linkage.[13,34] A peak was unique to only the NCs at 1735 cm^{-1}, with the peak assigned to the C=O stretching frequency of the sodium salt of carboxylic acid.[17] The FTIR results suggest that the C=O stretching vibration band of the CNs which appeared at 1735 cm^{-1} was due the oxidation process.

The values found for the content of negatively charged carboxylate groups through the conductometric titration were 0 and 1.7 mmol g^{-1} for CFs and CNs, respectively. These values confirm the incorporation of carboxylate groups into the cellulose chains after TEMPO-mediated oxidation.

The X-ray diffraction patterns for the CNs and CFs are shown in Figure 3. The CFs showed cellulose I characteristic peaks around $2\theta = 16.0°$ and 22.0°.[22] The 22.0° peak of the CNs became more intense, indicating increased perfection of the crystal lattice compared to its precursor. The analysis showed an increase in crystallinity from 69.0% for the CFs to 92.4% for the CNs, implying that the oxidation had a large effect on the destruction of amorphous regions of the cellulose. Highly crystalline CNs are more effective in achieving higher reinforcement for bionanocomposite in comparison to the CFs and CNs with lower crystallinity.[13]

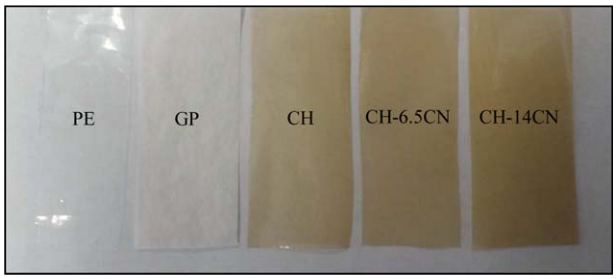

Figure 4. The visual appearance of PE, GP, pure chitosan, CH-6.5CN, and CH-14CN films. [Color figure can be viewed in the online issue, which is available at wileyonlinelibrary.com.]

Characteristics of the Films

Visual Appearance and Surface Morphology. The bionanocomposite films showed a slightly yellow appearance, whereas commercial PE and GP films were transparent and white, respectively (Figure 4).

TEM images of the bionanocomposite films are shown in Figure 5. As shown, the pure chitosan film [Figure 5(a)] showed a homogenous and continuous structure. The CH-6.5CN and CH-14CN films [Figure 5(b,c)] displayed a two-phase structure and random orientation of the CNs in the matrix, indicating good dispersion of nanocrystals in the bionanocomposite films. It is easy to observe the individual nanoparticle dispersion in the chitosan matrix and its small particle size. These results are a good indication of the excellent compatibility between the oxidized CNs and the chitosan matrix.

Mechanical Properties and Water-Vapor Permeability. Mechanical properties reflect the durability of films and their ability to enhance the mechanical integrity of foods.[4] Results of tensile strength (σ), elongation percentage at break point (ε), and Young's modulus (Y) of the different films are shown in Table I. The σ and Y values of the chitosan films increased significantly ($P \leq 0.05$) upon addition of CNs, which may be related to the nanofiller dispersion state and good interaction between the carboxylate groups of the CNs and cationic amino groups present in chitosan.[16,35] With increased CN content, σ and Y were improved by up to 136 and 224%, respectively, showing good reinforcing capacity of such nanocrystals in the chitosan matrix. In contrast, a decrease in ε with increasing amount of CNs was observed for films. This may be attributed to the rigid nature of the nanoparticles, which prevents motion of the polymer matrix.[13] The σ, ε, and Y values of developed bionanocomposite films were comparable to those of GP ($\sigma = 63.4 \pm 5.1$ MPa, $\varepsilon = 2.1\% \pm 0.3\%$, and $Y = 3760 \pm 619$ MPa) when used in sliced cheese interleaving. On the other hand, PE films were

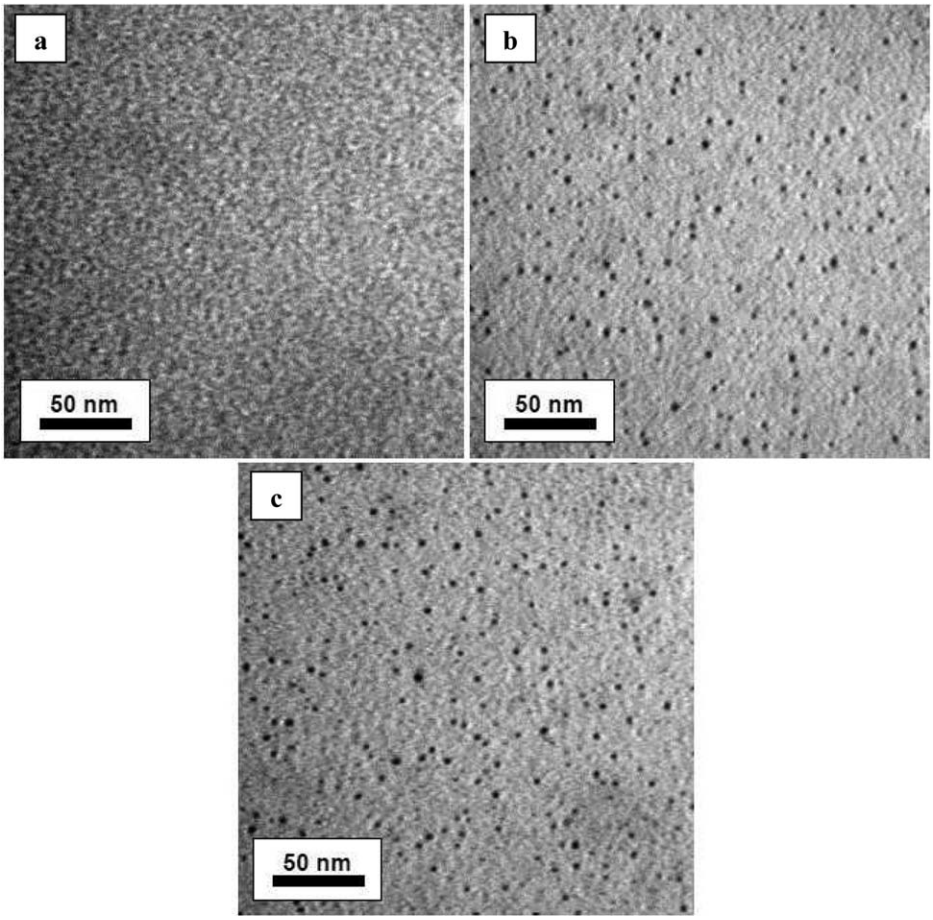

Figure 5. TEM images of films: (a) chitosan, (b) CH-6.5CN, and (c) CH-14CN.

significantly more extendible ($\varepsilon = 1100.6\% \pm 62.7\%$) and less resistant.

The effectiveness of polymer films is generally related to their mass-transport properties. The ability to decrease moisture transfer between the food and the surrounding atmosphere is critical for food quality and safety concerns.[36,37] Therefore, the study of water-vapor–barrier properties of a polymer film is of great importance for practical and commercial purposes. As can be seen in Table I, the incorporation of CNs in the chitosan matrix decreased the WVP by up to 70% compared with pure CH films [4.30×10^{-11} (g m^{-1} s^{-1} Pa^{-1})], wherein a higher efficiency was observed by increasing the proportion on CNs. Our hypothesis is that interactions between the negatively charged CNs and the cationic polymer matrix decrease the free volume and segmental motions, which increase the distance travelled by the water molecules to diffuse through the film, thus reducing the WVP.[4,13] Moreover, the high crystallinity of the CNs hampers the access of water to the internal structure.[35] The bionanocomposite films had a significantly ($P \leq 0.05$) lower WVP compared to that of GP and PE films, but it was on the same order of magnitude (10^{-11} g m^{-1} s^{-1} Pa^{-1}). The WVP of PE and GP films can range from 2.0×10^{-13} to 3.0×10^{-11} g m^{-1} s^{-1} Pa^{-1} [38–40] and from 3.9×10^{-11} to 8.6×10^{-10}

Table I. Properties of the Bionanocomposite Films of Chitosan–CNs

Film	*e* (μm)	σ (MPa)	ε (%)	*Y* (MPa)	*WVP* $\times 10^{-11}$ (g m^{-1} s^{-1} Pa^{-1})
CH	28.0 ± 1.0^{a}	32.0 ± 0.4^{a}	17.0 ± 0.4^{a}	2390 ± 376^{a}	4.30 ± 0.04^{a}
CH-6.5CN	28.0 ± 1.1^{a}	57.6 ± 0.9^{b}	4.9 ± 0.5^{b}	4365 ± 347^{b}	1.88 ± 0.06^{b}
CH-14CN	28.1 ± 1.3^{a}	76.3 ± 0.6^{c}	1.3 ± 0.5^{c}	8100 ± 596^{c}	1.28 ± 0.06^{c}
GP	44.3 ± 1.5^{b}	63.4 ± 5.1^{b}	2.1 ± 0.3^{c}	3760 ± 619^{b}	3.89 ± 0.09^{d}
PE	31.1 ± 1.3^{a}	11.9 ± 2.1^{d}	1100.6 ± 62.7^{d}	83.5 ± 17.7^{d}	2.91 ± 0.08^{e}

Mean values ± standard error (in triplicate). Different superscript letters in the same column indicate significant differences ($P \leq 0.05$) between the film properties. *e*: film thickness.

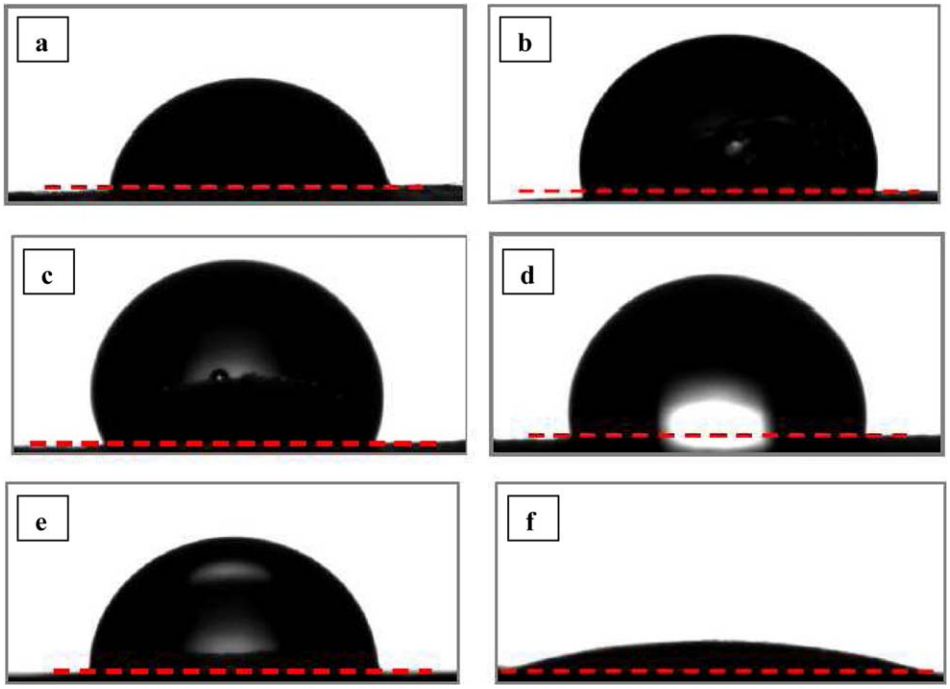

Figure 6. Water drops on the surfaces of films: (a) chitosan, (b) CH-6.5CN, (c) CH-14CN, (d) PE, (e) GP, and (f) sliced cheese. [Color figure can be viewed in the online issue, which is available at wileyonlinelibrary.com.]

g m^{-1} s^{-1} Pa^{-1},[41,42] respectively. These differences could be attributed to the incorporation of plasticizers or other additives in the film matrices during manufacture, which could alter the WVP values.

Hydrophobicity/Hydrophilicity, Surface Energy, and Adhesion. Figure 6 shows the profiles of water droplets on the surfaces of the evaluated films, and Table II shows the average values of the contact angle and surface energy values as well as the polar and dispersive energy components of the film surfaces.

From the results shown in Table II and Figure 6, there was an inverse relationship between the surface energy of the films and the contact angle of the droplets, indicating that the lower the surface energy, the lower the surface wettability of the films and, consequently, the greater the value of the contact angle.

Table II. Contact Angles and Surface Energies of the Films

Film	Contact angle (°)	Surface energy components (mJ m^{-2})		
		γ_S	γ_S^p	γ_S^d
CH	69.0 ± 0.6[a]	41.7	38.7	3.0
CH-6.5CN	107.8 ± 0.7[b]	34.9	13.1	21.8
CH-14CNO	115.3 ± 0.8[c]	29.0	3.4	25.6
PE	102.0 ± 0.8[d]	38.8	17.8	21.0
GP	90.8 ± 0.9[e]	39.2	19.0	20.2

Mean values ± standard error (in triplicate). Different superscript letters in the same column indicate significant differences ($P \leq 0.05$). γ_S: surface energy/tension of the films, γ_S^d: dispersive component of the solid surface tension, and γ_S^p: polar component of the solid (film) surface tension.

The θ values of the chitosan film were the smaller (69.0° ± 0.6°) [Figure 6(a) and Table II] and in agreement with the range found in previously published reports, that is, around 65°–70°,[43] which demonstrate the hydrophilic surface of the film ($\theta < 90°$). The higher hydrophilicity of the chitosan film can be attributed to the water-binding capacity of its functional groups (amino and hydroxyl groups). The θ values of all bionanocomposite films [Figure 6(b,c) as well as Table II] were >90°, so that the surface of the chitosan films after the incorporation of the CNs is considered to be predominantly hydrophobic. This may be attributed to the high crystallinity of the CNs and interactions among their anionic groups with the cationic groups present in the chitosan polymer chains. In this sense, the obtained results indicate that there may be a lesser amount of free amino and hydroxyl groups on the surface of bionanocomposite films, that is, the chitosan/CN interactions may have mobilized sites, which were used previously by water molecules, implying a decrease in the hydrophilic character of these materials. Similar results have been shown by other researchers with alginate[9] and starch.[10] As expected, the θ of the films of PE (102.0° ± 0.8°) and GP (90.8° ± 1.1°) were larger than 90°, indicating that the surfaces of these films, as well as the bionanocomposites, have hydrophobic character. The θ of sliced cheese was difficult to measure [Figure 6(f)], owing to the high affinity for water, as the drop spreads quickly over the surface of the cheese and almost formed a uniform film. These results are consistent with the results obtained for the WVP.

Analyzing the data in Table II, a variation in the values of polar and dispersive components of the surface energy of chitosan

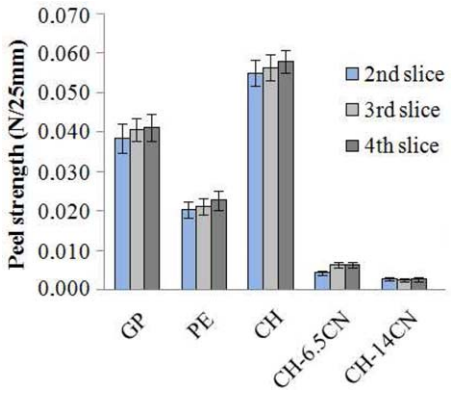

Figure 7. Peel test for the GP, PE, chitosan, CH-6.5CN, and CH-14CN films. [Color figure can be viewed in the online issue, which is available at wileyonlinelibrary.com.]

films after incorporation of CNs could be observed. The values of the polar components of the bionanocomposite films decreased, whereas the values of the dispersive components increased. Owing to a reduction in the values of the polar components, the interaction of water, a polar liquid, with the surface of the films becomes more difficult. Thus, the low wettability is justified and, consequently, the bionanocomposite films present greater hydrophobicity.

Adhesion between the surfaces of the cheese and the bionanocomposite films was evaluated through the peel test. The peel-strength results are shown in Figure 7.

As the data in Figure 7 show, regardless of the slice (second, third, or fourth), there were no significant differences between the peel strength values for the same film at the 95% confidence ($P > 0.05$). Commercial films, GP and PE, showed average peel-strength values of 0.03996 ± 0.0014 N/25 mm and 0.02138 ± 0.0012 N/25 mm, respectively. The pure chitosan films showed the highest peel-strength values (0.05634 ± 0.0014 N/25 mm), that is, the adhesion to the surface of the cheese was greater. With the incorporation of the CNs into the chitosan matrix, the peel-strength values decreased with increasing CN content. The CH-14CN films had the lowest mean value (0.0027 ± 0.0001 N/25 mm), which was about 21 times smaller than the value of the chitosan films. This may be attributed to its higher dispersive surface energy component (Table II), which makes the interaction between the surface of the films with polar groups (mainly of proteins and water) present on the surface of the cheese more difficult. From the results of surface energy and peel strength, it can be said that the adhesion is essentially related to the surface energy; the lower the surface energy (CH-14CN < CH-6.5CN < PE < PG < CH), the lower peel-strength value, indicating a decrease in the adhesive properties of the surface of the films.

CONCLUSIONS

This work shows that, by using the TEMPO-radical-mediated oxidation process combined with ultrasonic treatment, it was possible to obtain homogeneous and stable aqueous CN suspensions from corn cob fibers, which was evidenced by birefringence flow and confirmed by TEM analysis. The reinforcing CNs were well dispersed in the matrix of chitosan, which is a good indication of the excellent compatibility between the two components of the bionanocomposites films. The performances of the chitosan films were improved by CN reinforcement; the σ, Y, and WVP values were improved by up to 136, 224, and 70%, respectively, after oxidized CN addition to the chitosan matrix, showing good mechanical reinforcing capacity and barrier activity of such nanocrystals in the chitosan matrix. These properties are superior to those of the evaluated commercial interleaving films (PE and GP). The increase in contact angle and reduction in the surface energy of chitosan films after the incorporation of CNs indicated improvements in the hydrophobicity of the films. Furthermore, peel-test results showed that the bionanocomposite films had lower peel strengths, indicating lower adhesion to the sliced cheese surfaces compared to pure chitosan, PE, and GP films. These results suggest that the developed films may be exploited as food packaging, for example, as an interleaving film, owing to its excellent mechanical properties, permeability, hydrophobicity, and low surface adhesion.

ACKNOWLEDGMENTS

The authors thank CAPES (Brazilian Agency for Improvement of Graduate Personnel) for financial support. We would like to express our sincere thanks to the Process Control Laboratory (LCP) of UFSC for technical support during the contact angle measurements. The X-ray diffraction measurements were performed with Xpert MPD (MultiPurpose Diffractometer) of the LDRX-UFSC, Florianópolis, Brazil. The authors thank the LCME-UFSC for technical support during the microscopic analysis work.

REFERENCES

1. Khan, A.; Khan, R. A.; Salmieri, S.; Tien, C. L.; Riedl, B.; Bouchard, J.; Chauve, G.; Tan, V.; Kamal, M. R.; Lacroix, M. *Carbohydr. Polym.* **2012**, *90*, 1601.
2. Souza, V. C.; Monte, M. L.; Pinto, L. A. A. *Int. J. Food Sci. Technol.* **2013**, *48*, 1309.
3. Dotto, G. L.; Souza, V. C.; Pinto, L. A. A. *LWT Food Sci. Technol.* **2011**, *44*, 1786.
4. Souza, V. C.; Monte, M. L.; Pinto, L. A. A. *Int. J. Food Sci. Tech.* **2011**, *46*, 1856.
5. Ferreira, C. O.; Nunes, C. A.; Delgadillo,; Lopes da Silva, J. A. *Food Res. Int.* **2009**, *42*, 807.
6. Dufresne, A. In Monomers, Polymers and Composites From Renewable Resources; Gandini, A., Belgacem, M. N., Eds.; Elsevier: Oxford: **2008**; Chapter 19, p 401.
7. Dufresne, A. *Can. J. Chem.* **2008**, *86*, 484.
8. Rafieian, F.; Shahedi, M.; Keramat, J.; Simonsen, J. *Ind. Crop. Prod.* **2014**, *53*, 282.
9. Abdollahi, M.; Alboofetileh, M.; Behrooz, R.; Rezaei, M.; Miraki, R. *Int. J. Biol. Macromol.* **2013**, *54*, 166.
10. Cao, X. D.; Chen, Y.; Chang, P. R.; Stumborg, M.; Huneault, M. A. *J. Appl. Polym. Sci.* **2008**, *109*, 3804.

11. Pereda, M.; Dufresne, A.; Aranguren, M. I.; Marcovich, N. E. *Carbohydr. Polym.* **2014**, *101*, 1018.
12. Azeredo, H. M. C.; Mattoso, L. H. C.; Avena-Bustillos, R. J.; Filho, G. C.; Munford, M. L.; Wood, D.; Mchugh, T. H. *J. Food Sci.* **2010**, *75*, 1.
13. Souza, V. C.; Quadri, M. G. N. *J. Biobased Mater. Bioenergy* **2014**, *8*, 495.
14. Filson, P. B.; Dawson-Andoh, B. E. *Bioresour. Technol.* **2009**, *100*, 2259.
15. Flauzino Neto, W. P.; Silvério, H. A.; Dantas, N. O.; Pasquini, D. *Ind. Crop. Prod.* **2013**, *42*, 480.
16. Cao, X.; Ding, B.; Yu, J.; Al-Deyabd, S. S. *Carbohydr. Polym.* **2012**, *90*, 1075.
17. Benhamou, K.; Dufresne, A.; Magnin, A.; Mortha, G.; Kaddami, H. *Carbohydr. Polym.* **2014**, *99*, 74.
18. Silvério, H. A.; Neto, W. P. F.; Dantas, N. O.; Pasquini, D. *Ind. Crop. Prod.* **2013**, *44*, 427.
19. Ma, H.; Burger, C.; Hsiao, B. S.; Chu, B. *Biomacromolecules* **2011**, *12*, 970.
20. Fernandes, S. C. M.; Freire, C. S. R.; Silvestre, A. J. D.; Neto, C. P.; Gandinia, A.; Berglund, L. A.; Salmén, L. *Polymer* **2010**, *81*, 394.
21. Attila, O.; Julius, V. G. *Eur. Polym. J.* **2005**, *41*, 2803.
22. Segal, L.; Creely, L.; Martin, A. E.; Conrad, C. M. *Text. Res. J.* **1959**, *29*, 786.
23. ASTM. In Annual Book of American Standard Testing Methods; ASTM, Ed.; American Society for Testing and Materials: Philadelphia, PA, **2001**; p 162.
24. ASTM. In Annual Book of American Standard Testing Methods; ASTM, Ed.; American Society for Testing and Materials: Philadelphia, PA, **1995**; p 406.
25. Belyamani, I.; Prochazka, F.; Assezat, G.; Debeaufort, F. *Food Packag. Shelf Life* **2014**, *2*, 65.
26. Fowkes, F. M. *J. Phys. Chem.* **1962**, *66*, 1863.
27. Good, R. J.; van Oss, C. J. In The Modern Theory of Contact Angles and the Hydrogen Bond Components of Surface Energies; Schrader, M. E.; Loeb, G. I., Eds.; Plenum Press: New York, **1992**; Chapter 1, pp 1–27.
28. ASTM D3330. Standard Test Method for Peel Adhesion of Pressure-Sensitive Tape, ASTM International: West Conshohocken, PA, 2010, www.astm.org
29. Lu, H.; Gui, Y.; Zheng, L.; Liu, X. *Food Res. Int.* **2013**, *50*, 121.
30. Tischer, P. C. S. F.; Sierakowski, M. R.; Westfahl, H.; Tischer, C. A. *Biomacromolecules* **2010**, *11*, 1217.
31. Wang, S.; Cheng, Q. *J. Appl. Polym. Sci.* **2009**, *113*, 1270.
32. Marchessault, R. H.; Morehead, F. F.; Walter, N. M. *Nature* **1959**, *184*, 632.
33. Alemdar, A.; Sain, M. *Bioresour. Technol.* **2008**, *99*, 1664.
34. Sun, X. F.; Xu, F.; Sun, R. C.; Fowler, P.; Baird, M. S. *Carbohydr. Res.* **2005**, *340*, 97.
35. Mesquita, J. P. Nanocristais de celulose para preparação de bionanocompósitos com quitosana e carbonos nanoestruturados para aplicações tecnológicas e ambientais. Thesis (PhD in Chemistry)—Chemistry Department, UFMG, Belo Horizonte, Brazil, **2012**.
36. Khwaldia, K.; Basta, A. H.; Aloui, H.; El-Saied, H. *Carbohydr. Polym.* **2014**, *99*, 508.
37. Aloui, H.; Khwaldia, K.; Ben Slama, M.; Hamdi, M. *Carbohydr. Polym.* **2011**, *86*, 1063.
38. Dias, M. V.; Medeiros, H. S.; Soares, N. F. F.; Melo, N. R.; Borges, S. V.; Carneiro, J. D. S.; Pereira, J. M. T. A. K. *LWT Food Sci. Technol.* **2013**, *50*, 167.
39. Krochta, J. M. In Encyclopedia of Agricultural, Food and Biological Engineering; Heldman, D. R., Ed.; Marcel Dekker: New York: **2003**; p 720.
40. Smith, S. A. In The Wiley Encyclopedia of Packaging Technology; Bakker, M., Ed.; Wiley: New York: **1986**.
41. Larotonda, F. D. S.; Matsui, K. S.; Paes, S. S.; Laurindo, J. B. *Starch* **2003**, *55*, 504.
42. Debeaufort, F.; Voilley, A. *J. Agric. Food Chem.* **1994**, *42*, 2871.
43. Wanichapichart, P.; Sungkum, R.; Taweepreda, W.; Nisoa, M. *Surf. Coat. Technol.* **2009**, *203*, 2531.